Catalysis Today 146 (2009) 319–325

Contents lists available at ScienceDirect

Catalysis Today

journal homepage: www.elsevier.com/locate/cattod

Electrochemical promotion of CO conversion to CO_2 in PEM fuel cell PROX reactor

F.M. Sapountzi *, M.N. Tsampas, C.G. Vayenas

Department of Chemical Engineering, University of Patras, Caratheodory Str., 1, GR-26504 Patras, Greece

ARTICLE INFO

Article history:
Available online 11 June 2009

Keywords:
Electrochemical promotion (NEMCA)
PEM fuel cell
CO-poisoning
Gold
Platinum

ABSTRACT

The possibility of electrochemically promoting the water–gas-shift reaction and the CO oxidation reaction in a PEM fuel cell reactor supplied with a methanol reformate mixture was investigated in PEM fuel cells with Pt or Au state-of-the-art E-TEK anodes, in order to explore the use of PEMFC units as preferential oxidation of CO (PROX) reactors. The electropromotion of CO removal was investigated both with air or H_2 fed to the cathode side and also by O_2 bleeding to the anode during normal PEMFC operation. It was found that the catalytic activity of the anode for CO conversion to CO_2 can be modified significantly by varying the catalyst potential. The magnitude of the electrochemical promotion depends strongly on the anodic electrocatalyst (Pt or Au), on the CO concentration of the fuel mixture, on the operating temperature and on the presence of oxygen. The electropromotion effect and the Faradaic efficiency were found to be much higher in CO-rich anode environments.

1. Introduction

Electrochemical promotion of catalysis [1–20] (also known in the literature as NEMCA effect), is a phenomenon where non-Faradaic changes in the catalytic activity and selectivity are caused by the application of a small current or potential between a catalyst which is in contact with a solid electrolyte and a counter electrode deposited on the same electrolyte. In most cases, these changes are reversible, as they disappear upon interruption of the current or potential application. The effect of electrochemical promotion (EP) is due to an electrochemically induced and controlled migration (backspillover) of ions from the solid electrolyte to the catalytic metal/gas interface. These ions, accompanied by their compensating (screening) charge in the metal, form an effective electrochemical double layer on the gas-exposed catalyst surface. As a result, the catalyst work function changes and this affects the catalytic phenomena taking place there, in a very pronounced, reversible, and controlled manner [1–20].

PEM fuel cells are the most attractive of all the fuel cell types for many applications due to their simplicity, quick startup, efficiency, modularity and versatility, and therefore they are promising candidates for future portable, stationary and automotive applications [21,22]. The ideal fuel used in fuel cells is hydrogen, due its high reactivity and zero-emission characteristics. During hydrogen production via hydrocarbons or alcohol reforming, carbon monoxide is also formed. After cleaning up the reformate mixture, a small concentration of CO (10–100 ppm) remains in the mixture [21,22]. This small CO concentration is enough to cause a significant drop in PEM performance and power output, since CO binds strongly to the anodic electrocatalyst sites, resulting in the reduction of active surface sites available for hydrogen adsorption and thus hydrogen oxidation [23].

The purification of the stream can be achieved catalytically using the water–gas-shift (WGS) reaction

$$CO + H_2O \rightarrow CO_2 + H_2 \quad (1)$$

The WGS reaction is exothermic and thermodynamically limited, as high CO conversions can be obtained at low temperatures [24].

The preferential oxidation of CO (PROX) in presence of hydrogen is also a process used for the removal of CO from the hydrogen stream.

Therefore, the WGS and PROX systems have been studied intensively by many scientific groups for a plethora of catalytic systems [24–26].

In previous studies [27,28] it was found that electrochemical promotion of CO oxidation and of the water–gas-shift reaction on a Pt anode of a PEM fuel cell running under extreme CO-poisoning conditions (i.e. up to 5000 ppm CO) can be used in order to make methanol reformate mixtures suitable for anodic operation. It was also found [27,28] that the non-Faradaic behavior is strongly affected by the presence of oxygen.

The aim of this study was to examine the use of PEMFCs as PROX reactors and thus to explore if electrochemical promotion can enhance the rate of CO removal on nanodispersed Pt/C and Au/C anodes.

* Corresponding author. Tel.: +30 2610 997860; fax: +30 2610 997269.
E-mail address: fenia@chemeng.upatras.gr (F.M. Sapountzi).

0920-5861/$ – see front matter © 2009 Elsevier B.V. All rights reserved.
doi:10.1016/j.cattod.2009.04.024

2. Experimental

A PEM fuel cell unit provided by NuVant was used in the present work, similar to the one used in previous studies [27–29]. Two different membrane electrode assemblies (MEAs) of anode/electrolyte/cathode were constructed; Au/Nafion 117/Pt and Pt/Nafion 117/Pt. The Au and Pt electrodes were supported on E-TEK carbon cloth and had a metal loading of 3 mg Au/cm^2 and 0.5 mg Pt/cm^2, respectively. Nafion 117 with nominal thickness of 185 μm obtained from Dupont was used as the proton conductor. The membranes were prepared under hot-pressing conditions (under one metric ton, at 120 °C for 3 min). The electrode geometric surface area was in all cases 2.3 cm × 2.3 cm = 5.29 cm^2.

For the experiments run under extreme CO-poisoning conditions, a certified Messer–Griesheim dry gas mixture of 33.66% CO_2, 33.71% H_2, 0.63% CO and 31.98% N_2 was used at the anode, as used in previous studies [27,28]. The above fuel mixture was diluted with Messer–Griesheim He, in order to have several different gas compositions. We have labeled them according to their CO content as "700 ppm CO", "1150 ppm CO", "1500 ppm CO", "2050 ppm CO", "2400 ppm CO" and "2520 ppm CO". However, these fuel mixtures used differ not only in the CO content but also, proportionally, in the hydrogen concentration due to the dilution with He.

For the experiments run under mild CO-poisoning conditions, a certified Messer–Griesheim gas mixture containing 500 ppm CO diluted in H_2 was fed to the anode compartment and Air Liquide synthetic air was fed to the cathode. The anodic gas mixture could be further diluted with certified Messer–Griesheim pure H_2.

Both anode and cathode feeds were continuously humidified via thermostated gas saturators. All the experiments were carried out at 30 °C. The saturators temperature was set at 80 °C, which corresponds to partial pressure of water equal to 47.36 kPa, value required in order to simulate the stream with a methanol reformate mixture. The cell was maintained in a vertical position in order to minimize the effect of H_2O flooding at the anode. The flow rate for both anode and cathode feed was 170 cc/min during all the experiments.

For the application of constant currents or potentials to the cell, an AMEL 553 Galvanostat-Potentiostat was used. The analysis of the reaction products was carried out with a PERKIN-ELMER SIGMA 300 HWD Gas Chromatograph utilising a Molecular Sieve column to separate CO and H_2 and a Porapak N column to separate CO_2. For the continuous and quantitative measurement of CO and CO_2 concentration signals, a Fuji Electric's Infrared Analyzer ZRJ-4UNOR 6N IR CO/CO_2 analyzer was used.

3. Results and discussion

3.1. Morphology of the catalysts

Figs. 1 and 2 show the TEM images of the Au and Pt electrocatalysts, respectively. The Au electrode images are shown in Fig. 1a and b. The average diameter of the Au particles is clearly seen in these figures and was estimated to be 4.5 nm. The low magnification TEM image of the Pt electrode (Fig. 2a) shows the dispersion of the Pt particles on the carbon support, while in the highly magnified TEM image (Fig. 2b), the size of the Pt particles is clearly seen. The average diameter of the Pt particles was estimated to be 3 nm. Assuming particles with spherical geometry, and based on the particle diameter (as estimated from the TEM images), the superficial electrode surface area (5.29 cm^2), the density of each metal, and the metal loading of each electrode, one can calculate the real total surface area of each catalyst. All the above characteristics and the thus calculated values for the real total surface are given in Table 1 for both catalysts and all catalytic rates (r_s) presented here are normalized using these real total surface area values.

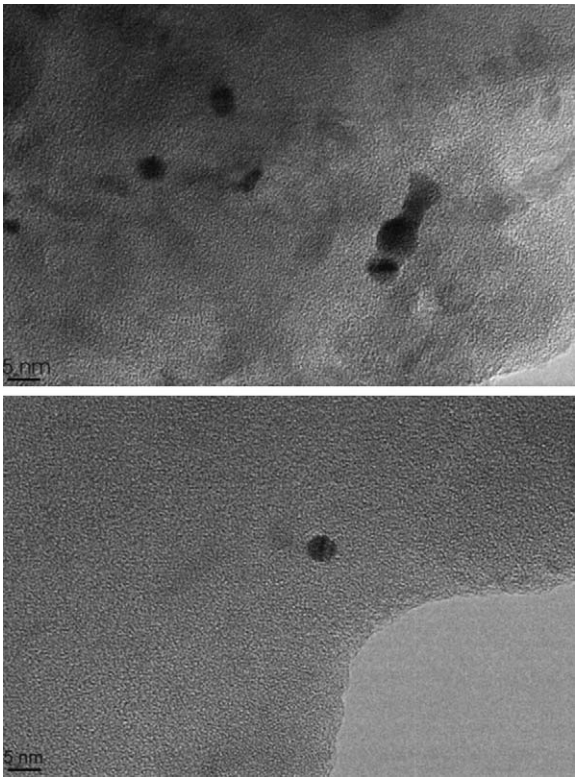

Fig. 1. (a and b) TEM images of the Au electrode. The black dots correspond to the metal particles.

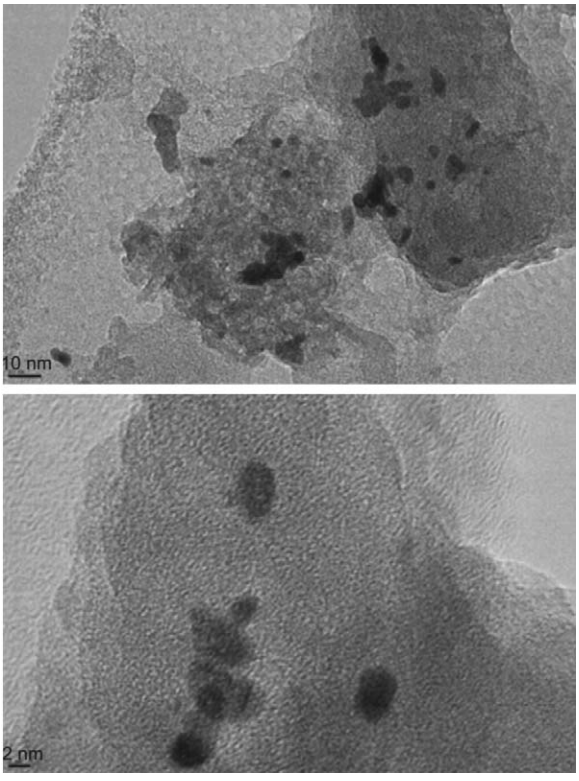

Fig. 2. (a and b) TEM images of different magnification of the Pt electrode. The black dots correspond to the metal particles.

Table 1
Characteristics of Pt and Au electrodes.

	Pt	Au
Geometric surface (cm^2)	5.29	5.29
Metal loading of electrode (mg/cm^2)	0.5	3.0
Metal density (g/cm^3)	21.4	19.3
Average particle diameter (nm)	3	4.5
Real total electrode surface (m^2)	0.25	1.05
Specific electrode surface (m^2/g)	93.5	66.1

3.2. Unpromoted catalytic activity

In previous studies [27,28], using a Pt anode, it was found that

(a) when the methanol reformate mixture is fed to the anode and hydrogen to the cathode of the cell, CO is consumed via the WGS reaction (1) while,
(b) when the methanol reformate mixture is fed to the anode and air to the cathode of the cell, oxygen can diffuse (crossover) through the Nafion membrane and CO is consumed not only due to the WGS reaction (1) but also due to direct CO oxidation

$$CO + \frac{1}{2}O_2 \rightarrow CO_2 \quad (2)$$

Fig. 3 compares the unpromoted catalytic activity (under open-circuit conditions) of a gold anode and a platinum anode, in terms of catalytic rate per real total surface area of each catalyst, running the cell under severe CO-poisoning conditions. The open symbols connected with the dashed line in Fig. 3 refer to the catalytic activity towards the water–gas-shift reaction (hydrogen supplied to the cathode). The closed symbols connected with the solid line in Fig. 3 refer to the catalytic activity towards both the water–gas-shift reaction and the CO oxidation (air supplied to the cathode).

As it is shown, the Au anode is catalytically more active than the Pt anode, with either air or hydrogen supplied to the cathode, when the cell operates under severe CO-poisoning conditions. It is worth reminding that since the different CO concentrations are obtained with dilution with He of the methanol reformate mixture, the concentration of H_2 in the feed was proportionally different too (the ratio p_{CO}/p_{H_2} was equal to 0.0187 in all cases).

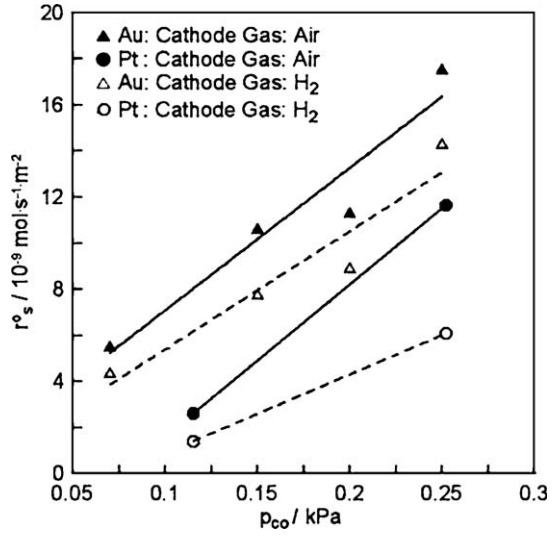

Fig. 3. The catalytic rate per real total surface area of each catalyst under open-circuit conditions over a range of p_{CO} in the fuel mixture, when the cell operates under extreme CO-poisoning conditions (methanol reformate supplied to the anode). The open symbols connected with the dashed line refer to catalytic activity towards the water–gas-shift reaction, as hydrogen was supplied to the cathode. The closed symbols connected with the solid line refer to catalytic activity towards both the water–gas-shift reaction and the CO oxidation, as air was supplied to the cathode.

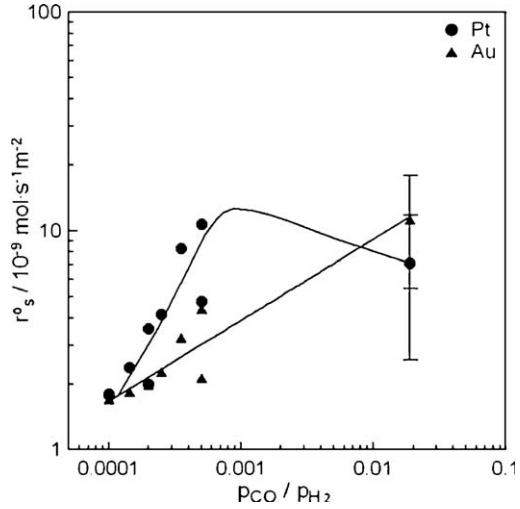

Fig. 4. The catalytic rate per real total surface area of each catalyst under open-circuit conditions over a wide range of the ratio p_{CO}/p_{H_2} in the fuel mixture (both mild and severe CO-poisoning). We refer to catalytic activity both for WGS and CO oxidation, since data refer to the case of supplying air to the cathode. Gold is catalytically more active when the cell operates under extreme CO-poisoning conditions, while Pt is more active when the cell operates under mild CO-poisoning conditions.

The role of oxygen crossover on the catalytic rate of CO consumption is clearly shown in this figure, since the catalytic rate is larger in presence of oxygen (air at the cathode). To be more specific, in the case of the Au anode, the rate of CO consumption is 1.3 times larger when air is fed to the cathode. This implies that roughly 75% of the CO consumed on the Au anode is due to the water–gas-shift reaction, and the remaining 25% is due to CO oxidation. Using the Pt anode, the rate of CO consumption is two times larger in presence of oxygen at the cathodic compartment, indicating that typically half of the CO consumed at the Pt anode corresponds to the water–gas-shift reaction, and the remaining half to the direct CO oxidation.

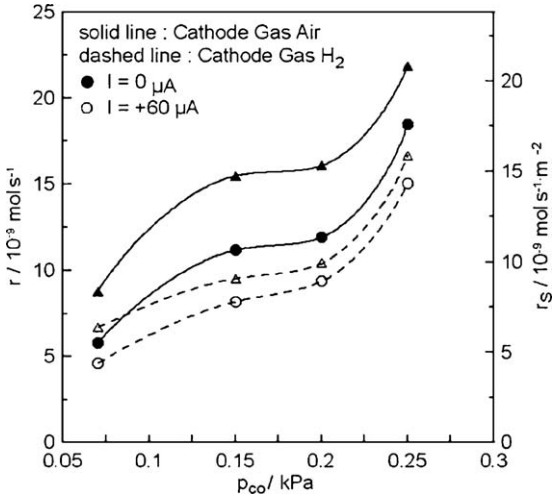

Fig. 5. Effect of application of a positive current of 60 μA (H^+ transport from the anode to the cathode) on the catalytic rate of CO consumption (r) and on the catalytic rate per real total surface (r_s), when oxygen is supplied to the cathode (solid line) and when hydrogen is supplied to the cathode (dashed line) using the gold anode.

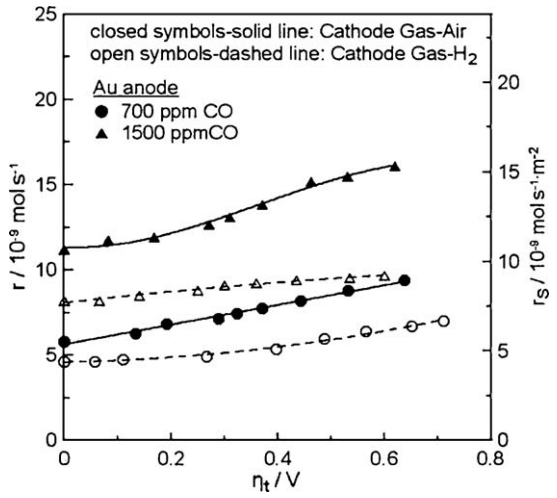

Fig. 6. The effect of total overpotential on the catalytic rate of CO consumption (r) and on the catalytic rate per real total surface area (r_s) for the gold anode under extreme CO-poisoning conditions, in presence of air at the cathode (closed symbols-solid line) and in presence of hydrogen at the cathode (open symbols-dashed line).

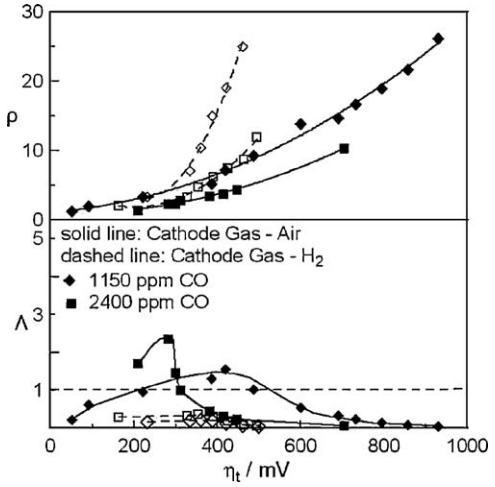

Fig. 8. The effect of total overpotential on the parameters ρ and Λ for two different methanol reformate mixtures (extreme CO-poisoning), in presence of air in the cathode (solid line) and in presence of hydrogen in the cathode (dashed line) using the platinum anode.

The high catalytic activity of gold (higher than that for platinum) has also been reported in the literature, in the case of nanodispersed gold particles (<5 nm), and generally it is well documented that the catalytic properties of gold depend strongly on the type of the support [24,26,30–38].

Fig. 4 gives a comparison of the catalytic activity over a wide range of CO concentrations (both severe and mild poisoning of CO). These data refer to catalytic activity for both reactions (1) and (2), since air was supplied to the cathode. As already mentioned, the values of the catalytic rate in the case of extreme CO-poisoning conditions correspond to the same value of p_{CO}/p_{H_2}. For this reason, in Fig. 4 the mean average of these rate values are given for $p_{CO}/p_{H_2} = 0.0187$ (error bars are also shown).

As discussed above, under severe contamination (large p_{CO}/p_{H_2} values) the gold anode is more active than the platinum anode. However, as shown in Fig. 4, different behavior is observed under mild CO-poisoning conditions (small p_{CO}/p_{H_2} values), since higher reaction rates of CO consumption were obtained with the Pt anode. This observation is in agreement with the literature, where it is

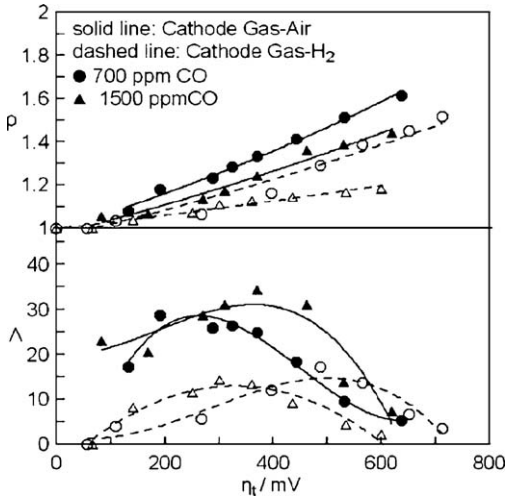

Fig. 7. The effect of total overpotential on the parameters ρ and Λ for two different methanol reformate mixtures (extreme CO-poisoning), in presence of air in the cathode (solid line) and in presence of hydrogen in the cathode (dashed line) using the gold anode.

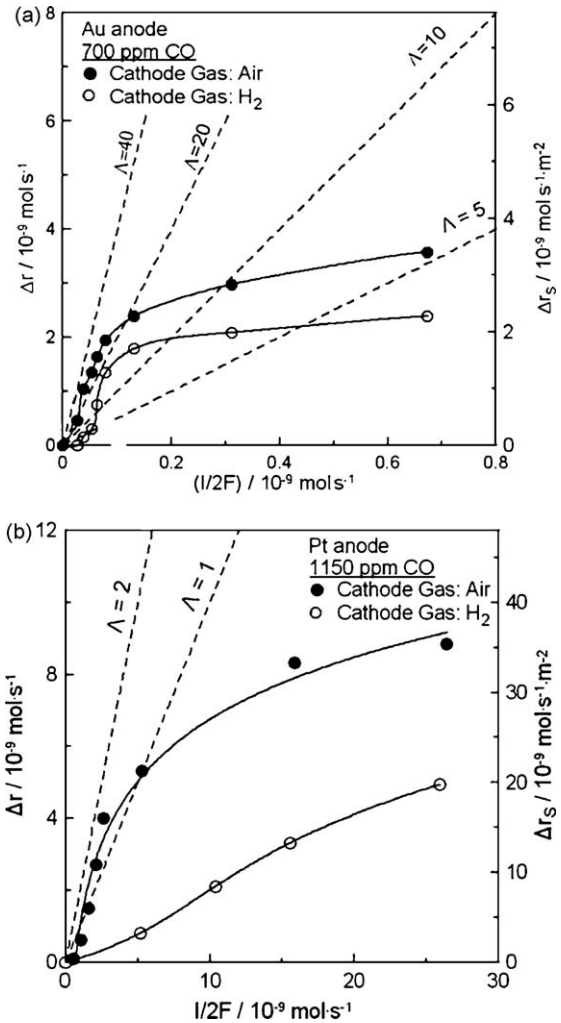

Fig. 9. The effect of the rate of H_2 transport from the anode to the cathode ($I/2F$) on the increase in the catalytic rate (Δr) and on the increase in the catalytic rate per real total surface area (Δr_s) when air or hydrogen is supplied to the cathode for the gold anode (a) and the platinum anode (b), for operation under severe contamination of CO.

mentioned that gold is more active for the removal of CO when mixtures with high CO concentration are supplied to the anode, while platinum is more active when the anode feed contains lower CO concentration [39].

With the Pt anode, it appears that a volcano behavior exists for the unpromoted catalytic rate and the ratio p_{CO}/p_{H_2}. The maximum may corresponds to half coverage of the Pt anode by CO as envisioned in Langmuir–Hinshelwood kinetics (Fig. 4). On the other hand, since CO is adsorbed weakly on gold, the catalytic rate is increased with increasing the ratio p_{CO}/p_{H_2} for the case of the Au anode (Fig. 4).

3.3. Electrochemical promotion of the catalytic activity

As shown in Fig. 5, using the gold anode, application of a positive current (protons transport from the anode to the cathode) of 60 μA leads to enhancement in the catalytic rate of CO consumption, r, and on the catalytic rate per real total surface, r_s, both when oxygen is supplied to the cathode (solid line in figure) and when hydrogen is supplied to the cathode (dashed line in figure). Fig. 6 shows the effect of application of different values of total (anodic and cathodic) overpotential (η_t) to the Au/Nafion 117/Pt cell on the catalytic rate r, and on the catalytic rate per real total surface area, r_s.

The magnitude of the enhancement in catalytic activity observed in Figs. 5 and 6, can be expressed by introducing the parameters ρ (rate enhancement ratio) and Λ (Faradaic efficiency), defined from

$$\rho = \frac{r}{r_o} \tag{3}$$

$$\Lambda = \frac{\Delta r}{I/2F} \tag{4}$$

where r is the electrochemically promoted catalytic rate and r_o the unpromoted catalytic rate, Δr is the change in the catalytic rate caused by the current or potential application, I is the applied current and F is the Faraday's constant. All the catalytic rates (r) are expressed as mol CO/s, thus we use $I/2F$ in (4). When $|\Lambda| \geq 1$, the changes in the catalytic rate are non-Faradaic and the reaction exhibits NEMCA behavior, while pure electrocatalysis dominates when $|\Lambda| < 1$ [1].

In these terms, a quantitative description of the enhancement in the catalytic activity is given in Fig. 7. This figure shows the effect of total overpotential (η_t) on the parameters ρ and Λ for two different fuel mixtures with high CO concentration (extreme CO-poisoning), both when the cathode gas is air (solid line in figure) and when the cathode gas is hydrogen (dashed line in figure) using the gold anode. All the changes observed under extreme CO-poisoning conditions are non-Faradaic, since Λ values much higher than unity (up to 40) were obtained. The non-Faradaic effect is more pronounced (larger Λ values) in

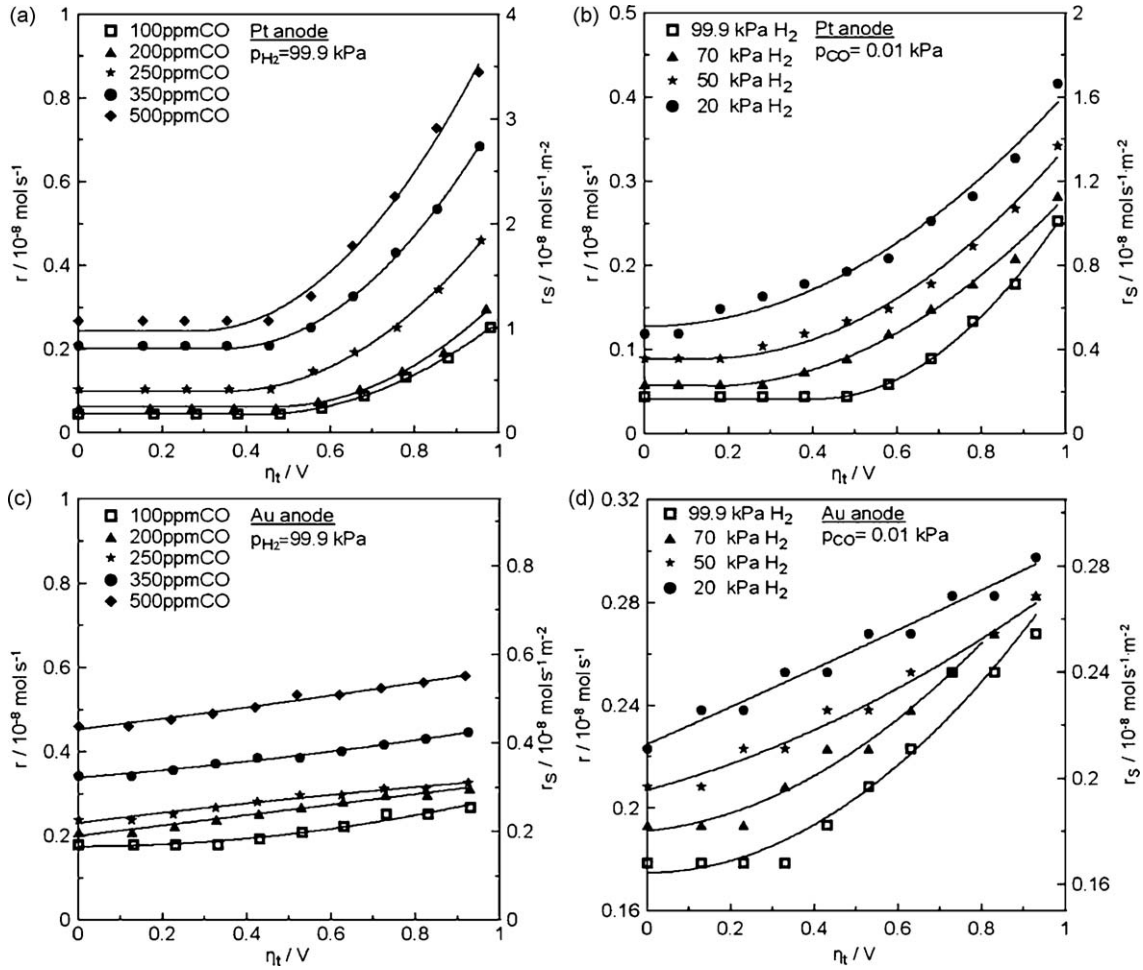

Fig. 10. The effect of anodic polarization (total overpotential) on the catalytic rate (r) and on the catalytic rate per real total surface area (r_s) under mild CO-poisoning conditions either keeping the p_{H_2} equal to 99.9 kPa and varying the CO concentration from 100 to 500 ppm (a and c) or and keeping the p_{CO} equal to 0.01 kPa and varying the p_{H_2} from 20 to 99.9 kPa (b and d) in the case of Pt anode (a and b) and in the case of the Au anode (c and d).

presence of oxygen at the cathode feed, showing that oxygen crossover through the Nafion membrane has a promoting role. Moreover, a maximum of Λ is observed at intermediate values of total overpotential.

Fig. 8 shows the effect of total overpotential on the parameters ρ and Λ for two different fuel mixtures with high CO concentration (extreme CO-poisoning), both when the cathode gas is air (solid line in figure) and when the cathode gas is hydrogen (dashed line in figure) using the platinum anode [27,28]. In presence of oxygen at the cathode, the changes in the catalytic rate are non-Faradaic (Λ values larger than unity), while in the case of hydrogen feeding to the cathode, the changes observed are totally sub-Faradaic (Λ values lower than unity).

Fig. 9 shows the effect of the rate of H_2 removal from the anode ($I/2F$) on the increase in the catalytic rate (Δr) and on the increase in the catalytic rate per real total surface area (Δr_s), both when air or hydrogen is supplied to the cathode. Fig. 9a refers to the gold anode and Fig. 9b to the platinum anode. The dashed lines in the figures correspond to constant Λ values. The promoting effect of the presence of oxygen at the cathode is clearly shown in these figures (larger Λ values when air is fed to the cathode). Moreover, it is observed that the non-Faradaic behavior is more pronounced in the case of the gold anode.

The effect of anodic polarization on the catalytic rate r and on the catalytic rate per real total surface r_s was also examined both for Au and Pt anodes, under mild CO-poisoning conditions. Kinetic experiments were carried out, keeping the p_{H_2} equal to 99.9 kPa and varying the CO concentration from 100 to 500 ppm, and also keeping the p_{CO} equal to 0.01 kPa and varying the p_{H_2} from 20 to 99.9 kPa. The results for the Pt anode are shown in Fig. 10a and b, where the effect of total overpotential (η_t) on the catalytic rate of CO consumption is shown. The changes observed upon polarization under mild CO-poisoning conditions were lower than those observed under extreme CO-poisoning conditions, and they were totally sub-Faradaic (Λ did not exceed unity under mild CO-poisoning conditions, as discussed earlier). Similar results were obtained with the Au anode (Fig. 10c and d). In this case (Fig. 10d) the data seem to converge to an isokinetic point near η_{fc} = 1 V for the various p_{H_2} values.

Figs. 11 and 12 give a comparison of the magnitude of electrochemical promotion of the catalytic activity for Au and Pt, over a wide range of fuel concentration. Fig. 11a and b present the dependence of ρ on the ratio p_{CO}/p_{H_2} and show that ρ exhibits a minimum in the case of Pt (Fig. 11b) which is not very clear in the case of Au (Fig. 11a). The overall enhancement in the catalytic rate is more pronounced when the Pt anode is used, since ρ values are one order of magnitude larger than that obtained with the Au anode, over the whole range of p_{CO}/p_{H_2} ratio examined (Fig. 11a and b).

Fig. 12 represents a log–log plot of Λ vs. p_{CO}/p_{H_2}. One observes that Λ increases when the ratio p_{CO}/p_{H_2} increases, and exceeds unity only under extreme CO-poisoning conditions (i.e. small p_{H_2} or large p_{CO} values). Additionally, it is observed that for all the gas mixture concentrations examined, the Faradaic efficiency Λ is larger in the case of the Au anode. This is mainly because the exchange current I_o for Pt was found to be [40] larger in a factor of 10 than that for Au, which is consistent with the superior performance of Pt electrodes in PEMFC units [21].

The slopes in Fig. 12 are approximately equal to unity for both anodic electrocatalysts (specifically the slope is 1.2 for Pt and 1.1 for Au), indicating linear dependence between Λ and p_{CO}/p_{H_2}, which can be rationalized [1] by the electrochemical promotion equation

$$\Lambda_{theor} = \frac{2Fr_o}{I_o} \quad (5)$$

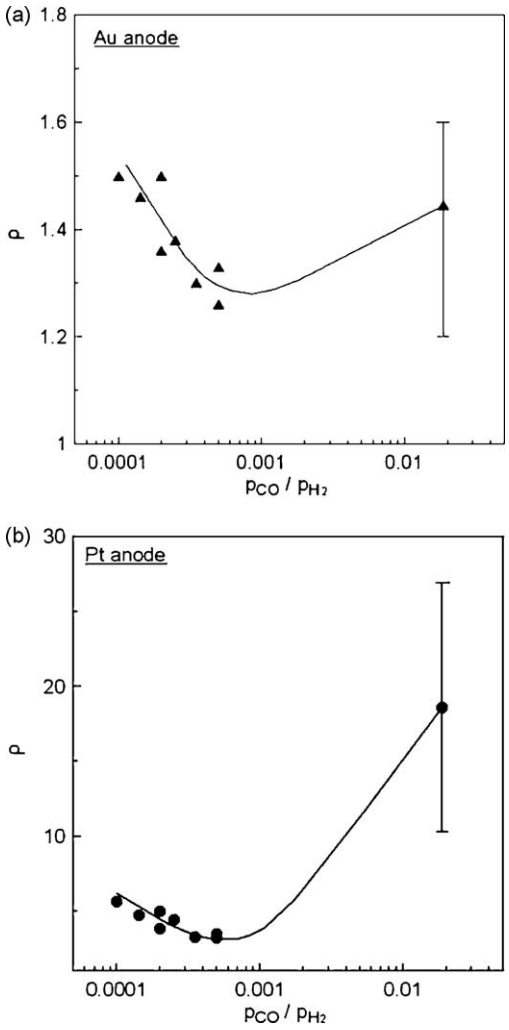

Fig. 11. Rate enhancement ratio, ρ, over a wide range of the ratio p_{CO}/p_{H_2} for Au anode (a) and Pt anode (b).

where r_o is the unpromoted catalytic rate which can be reasonably assumed to be proportional to θ_{CO} and I_o is the exchange current of the electrocatalytic reaction which is nearly proportional to p_{H_2}.

As discussed above, the presence of oxygen can enhance significantly the non-Faradaic behavior. However, this enhance-

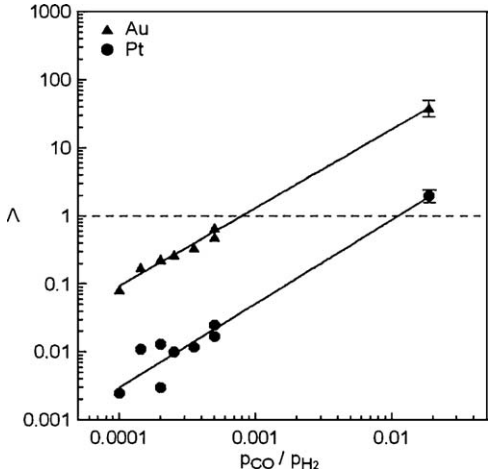

Fig. 12. The Faradaic efficiency, Λ, dependence on the ratio p_{CO}/p_{H_2} for the Au and the Pt anode, in the form of log–log plot.

ment is pronounced only when the ratio p_{CO}/p_{H_2} in the feed is quite large. At elevated values of p_{H_2}, the non-Faradaic effect is diminished.

4. Conclusions

The catalytic activity for CO removal of platinum and gold anodes of a PEM fuel cell was examined. CO is consumed via the water–gas-shift reaction when hydrogen is supplied to the cathode of the cell. The rate of CO consumption is significantly enhanced when air is supplied to the cathode of the cell, due to oxygen permeation (crossover) across the Nafion membrane, leading to direct CO oxidation. Gold is catalytically more active to remove CO than Pt, when the cell operates under extreme CO-poisoning conditions, while Pt is more active when the fuel mixture is rich in hydrogen and contains traces of CO.

Electrochemical removal of H^+ from the anode leads to enhancement in the catalytic rate. The changes observed were non-Faradaic (Λ up to 40 for Au, Λ up to 2.5 for Pt). The magnitude of electrochemical promotion is influenced by the presence of oxygen and by the ratio p_{CO}/p_{H_2} contained in the fuel mixture, in agreement with the expression

$$\Lambda_{theor} = \frac{2Fr_o}{I_o}$$

In general, it was found that NEMCA is more pronounced in the case of gold anodes, in presence of oxygen at the cathode side and for CO-rich anode environments.

Acknowledgements

We thank Dr. S. Balomenou and Dr. D. Tsiplakides (CERTH/CPERI) for the TEM images, and Professor E. Smotkin and his company, NuVant, for supplying us with the state-of-the-art PEMFC unit.

References

[1] C.G. Vayenas, S. Bebelis, C. Pliangos, S. Brosda, D. Tsiplakides, Electrochemical Activation of Catalysis: Promotion, Electrochemical Promotion and Metal-Support Interactions, Kluwer Academic/Plenum Publishers, New York, 2001.
[2] C.G. Vayenas, S. Bebelis, S. Ladas, Nature 343 (1990) 625.
[3] M. Stoukides, C.G. Vayenas, J. Catal. 70 (1981) 137.
[4] C.G. Vayenas, S. Bebelis, S. Neophytides, J. Phys. Chem. 92 (1988) 5083.
[5] T.I. Politova, V.A. Sobyanin, V.D. Belyaev, React. Kinet. Catal. Lett. 41 (1990) 321.
[6] N.A. Anastasijevic, H. Baltruschat, J. Heitbaum, Electrochim. Acta 38 (1993) 1067.
[7] S. Bebelis, C.G. Vayenas, J. Catal. 118 (1989) 125.
[8] J. Pritchard, Nature (London) 343 (1990) 592.
[9] R. Lambert, in: A. Wieckowski, E.R. Savinova, C.G. Vayenas (Eds.), Catalysis and Electrocatalysis at Nanoparticle Surfaces, Marcel Dekker Inc., New York, 2003.
[10] L. Ploense, M. Salazar, B. Gurau, E.S. Smotkin, JACS 119 (1997) 11550.
[11] Ch. Kokkofitis, G. Karagiannakis, S. Zisekas, M. Stoukides, J. Catal. 234 (2005) 476.
[12] N. Kotsionopoulos, S. Bebelis, J. Appl. Electrochem. 35 (2005) 1253.
[13] E. Lamy-Pitara, S.E. Mouahid, J. Barbier, Electrochim. Acta 45 (2000) 4299.
[14] S. Neophytides, D. Tsiplakides, P. Stonehart, M. Jaksic, C.G. Vayenas, Nature (London) 370 (1994) 292.
[15] I.M. Petrushina, V.A. Bandur, F. Cappeln, N.J. Bjerrum, J. Electrochem. Soc. 147 (2000) 3010.
[16] C. Cavalca, G. Larsen, C.G. Vayenas, G. Haller, J. Phys. Chem. 97 (1993) 6115.
[17] X. Li, F. Gaillard, P. Vernoux, Top. Catal. 44 (2007) 391.
[18] G. Pacchioni, F. Illas, S. Neophytides, C.G. Vayenas, J. Phys. Chem. 100 (1996) 16653.
[19] I. Riess, C.G. Vayenas, Solid State Ionics 159 (2003) 313.
[20] A. Jaccoud, C. Falgairette, G. Fóti, Ch. Comninellis, Electrochim. Acta 52 (2007) 7927.
[21] F. Barbir, in: Nigel Sammes (Ed.), PEM Fuel Cells, in Fuel Cell Technology: Reaching Towards Commercialization, Springer-Verlag London Ltd., Germany, 2006.
[22] K.S. Bhambare, S. Gupta, M.M. Mench, A. Ray, Sens. Actuat. B: Chem. 134 (2008) 803.
[23] X. Cheng, Z. Shi, N. Glass, L. Zhang, J. Zhang, D. Song, Z.-S. Liu, H. Wang, J. Shen, J. Power Sources 165 (2007) 739.
[24] R. Burch, Phys. Chem. Chem. Phys. 8 (2006) 5483.
[25] C.W. Corti, R.J. Holliday, D.T. Thompson, Appl. Catal. A: Gen. 291 (2005) 253.
[26] D. Cameron, R. Holliday, D. Thompson, J. Power Sources 118 (2003) 298.
[27] F.M. Sapountzi, M.N. Tsampas, C.G. Vayenas, Catal. Today 127 (1–4) (2007) 295.
[28] F. Sapountzi, M.N. Tsampas, C.G. Vayenas, Top. Catal. 44 (3) (2007) 461.
[29] R. Liu, E.S. Smotkin, J. Electroanal. Chem. 535 (2002) 49.
[30] G.C. Bond, D.T. Thompson, Catal. Rev.: Sci. Eng. 41 (3–4) (1999) 319.
[31] N. Weiher, E. Bus, L. Delannoy, C. Louis, D.E. Ramaker, J.T. Miller, J.A. van Bokhoven, J. Catal. 240 (2006) 100.
[32] J.R. Mellor, A.N. Palazov, B.S. Grigorova, J.F. Greyling, K. Reddy, M.P. Letsoalo, J.H. Marsh, Catal. Today 72 (2002) 145.
[33] M. Haruta, Catal. Today 36 (1997) 153.
[34] T.V. Choudhary, D.W. Goodman, Appl. Catal. A: Gen. 291 (2005) 32.
[35] T. Tabakova, V. Idakiev, K. Tenchev, F. Boccuzzi, M. Manzolo, A. Chiorino, Appl. Catal. B: Environ. 63 (2006) 94.
[36] A. Sandoval, A. Gómez-Cortés, R. Zanella, G. Díaz, J.M. Saniger, J. Mol. Catal. A: Chem. 278 (2007) 200.
[37] M. Haruta, M. Daté, Appl. Catal. A: Gen. 222 (2001) 427.
[38] S. Kandoi, A.A. Gokhale, L.C. Grabow, J.A. Dumesic, M. Mavrikakis, Catal. Lett. 93 (2004) 93.
[39] M. Haruta, S. Tsubota, in: A. Wieckowski, E.R. Savinova, C.G. Vayenas (Eds.), Catalysis and Electrocatalysis at Nanoparticle Surfaces, Marcel Dekker Inc., New York, 2003.
[40] F.M. Sapountzi, PhD Thesis, University of Patras, 2009.